Atmos. Chem. Phys. Discuss., https://doi.org/10.5194/acp-2018-196
Manuscript under review for journal Atmos. Chem. Phys.
Discussion started: 23 February 2018

Atmospheric Chemistry and Physics Discussions

Molecular and physical characteristics of aerosol at a remote marine free troposphere site: Implications for atmospheric aging

Simeon K. Schum[1], Bo Zhang[2,a], Katja Dzepina[1,b], Paulo Fialho[3], Claudio Mazzoleni[2,4] and Lynn R. Mazzoleni[1,2]

[1]Department of Chemistry, Michigan Technological University, Houghton, MI, USA
[2]Atmospheric Science Program, Michigan Technological University, Houghton, MI, USA
[3]Institute for Volcanology and Risk Assessment – IVAR, University of the Azores, Angra do Heroísmo, Portugal
[4]Department of Physics, Michigan Technological University, Houghton, MI, USA
[a]now at the National Institute of Aerospace, Hampton, VA, USA
[b]now at the Department of Biotechnology, University of Rijeka, Croatia

Correspondence to: Lynn R. Mazzoleni (lrmazzol@mtu.edu)

Abstract. Aerosol properties are transformed by atmospheric processes during long-range transport and play a key role in the Earth's radiative balance. To understand the molecular and physical characteristics of free tropospheric aerosol, we studied samples collected at the Pico Mountain Observatory in the North Atlantic. The observatory is located in the marine free troposphere at 2225 m above sea level, on Pico Island in the Azores archipelago. The site is ideal for the study of long-range transported free tropospheric aerosol with minimal local influence. Three aerosol samples with elevated organic carbon concentrations were selected for detailed analysis. FLEXPART retroplumes indicated that two of the samples were influenced by North American wildfire emissions transported in the free troposphere and one by North American outflow mainly transported within the marine boundary layer. To determine the molecular composition of the samples, we used ultrahigh resolution Fourier transform ion cyclotron resonance mass spectrometry. Thousands of molecular formulas were assigned to each of the individual samples. On average ~60 % of the molecular formulas contained only carbon, hydrogen, and oxygen atoms (CHO), ~30 % contained nitrogen (CHNO), and ~10 % contained sulfur (CHOS). The molecular formula composition of the two wildfire influenced aerosol samples transported mainly in the free troposphere had relatively low average O/C ratios (0.46 ± 0.12 and 0.47 ± 0.15) despite 7 - 10 days of transport time according to FLEXPART. However, the molecular composition of the North American outflow transported mainly in the boundary layer had a higher average O/C ratio (0.55 ± 0.19) with 3 days of transport time. Thus, aerosol oxidation appears to be related to environmental factors during transport and not simply aging time. Meteorological conditions extracted from GFS analysis for model grids along the FLEXPART simulated transport pathways and the observed molecular chemistry were used to predict the phase state of the aerosol samples, indicating that the aerosol transported in the free troposphere was more likely to be solid and therefore less oxidized than the aerosol transported in the boundary layer. This suggests that biomass burning emissions injected into the free troposphere are longer-lived than emissions in the boundary layer.

1 Introduction

Atmospheric organic aerosol composition and mass concentrations are transformed by atmospheric processes including oxidization (Dunlea et al., 2009; Jimenez et al., 2009; Kroll et al., 2011), cloud processing (Ervens et al., 2007, 2011; Zhao et al., 2013), and wet or dry deposition (Pöschl, 2005). Oxidation of organic aerosol impacts aerosol lifetime and aerosol-cloud interactions, including cloud droplet and ice nucleation (Massoli et al., 2010; Lambe et al., 2011; China et al., 2017), aerosol morphology, and optical properties (Pöschl, 2005; China et al., 2015; Laskin et al., 2015 and references therein). As such, the chemistry of atmospheric aerosol oxidation has received much attention (George and Abbatt, 2010; Lee et al., 2011; Kroll et al., 2011). Changes in the oxidation of anthropogenic organic aerosol emitted from Mexico City as it was transported

downwind was studied by Jimenez et al. (2009). They used an aerosol mass spectrometer (AMS) instrument on board an aircraft to measure the magnitude of the *m/z* 44 fragment as a proxy for the oxidation of organic aerosol in an AMS. After 6 hours and 63 km of transport, a noticeable increase in the overall chemical oxidation was observed. Rapid oxidation was also observed using an AMS in studies of biomass burning organic aerosol in Africa (Capes et al., 2008; Vakkari et al., 2014) and over the Mediterranean Sea (Bougiatioti et al., 2014). These analyses found that most of the marker species for biomass burning had been oxidized within 24 hours (Vakkari et al., 2014), suggesting that after 24 hours organic aerosol is nearly indistinguishable regardless of source. Except for the study by Capes et al. (2008) the aerosol in these studies was generally collected relatively close (< 30 hours downwind, mostly < 10 hours) to the emission sources. These studies all show the importance of oxidation to the aging of organic aerosol and provide motivation for studies of the oxidation of long-range transported organic aerosol.

A study of predominately Asian anthropogenic aerosol transported in the free troposphere over the Pacific Ocean found that the oxidation, inferred by the average oxygen to carbon ratio (O/C), continued to increase over the course of roughly a week (Dunlea et al., 2009). In a study biomass burning aerosol transported in the free troposphere across the North Atlantic Ocean, Dzepina et al. (2015) observed a relatively low O/C ratio (0.46 ± 0.13), considering the aerosol transport time of more than 10 days (Aiken et al., 2008). The authors hypothesized that cloud processing and other oxidative processes led to the formation and subsequent removal of oxidized species, leaving behind the long-lived aerosol species. Recent studies of long-range transported brown carbon (BrC) from biomass burning found that the aging of aerosol led to a near complete depletion of BrC within 24 hours (Forrister et al., 2015; Laing et al., 2016). The remaining BrC was found to lead to a 6 % increase of BrC over background levels and may represent the ubiquitous BrC present in the atmosphere far from the source (Forrister et al., 2015). This leftover BrC aerosol could impact large areas globally because much of it is located within the free troposphere and above clouds, due to the typically elevated injection heights of aerosol over wildfires (Val Martin et al., 2008a). These studies indicate that free tropospheric aerosol chemistry is particularly important because this aerosol can have a longer atmospheric lifetime than boundary layer aerosol (Laing et al., 2016) allowing it to be transported over greater distances.

Most studies of transported biomass burning aerosol are performed using instrumentation onboard aircrafts (Capes et al., 2008), at low altitude sites (Bougiatioti et al., 2014; Vakkari et al., 2014), or at continental mountain sites (Laing et al., 2016). Aircraft measurements have the advantage of sampling aerosol over wide spatial and altitudinal ranges, but they are limited to short time periods, typically of a few days to a week (Capes et al., 2008; Dunlea et al., 2009). Ground sites are less constricted by time, but because of the high injection heights, biomass burning aerosol are often above the boundary layer (Val Martin et al., 2008a). Thus, low altitude sites are less often affected by these plumes. Continental mountain sites typically have seasonally limited access to the free troposphere, because high summer temperatures can lead to planetary boundary layer influence through convection (Collaud Coen et al., 2011). Thus, many of the continental mountain sites have access to the free troposphere in the winter, but not in the summer when most wildfire activity occurs. The Pico Mountain Observatory (PMO, see the Supplement for additional information), is located 2225 m above sea level (a.s.l) within the caldera of Pico Mountain, on Pico Island in the Azores archipelago in the North Atlantic. The marine boundary layer in the region has been measured and estimated to range from 500 to 2000 m a.s.l in the summer months (Kleissl et al., 2007; Remillard et al., 2012; Zhang et al., 2017), well below the PMO. This allows access to free tropospheric long-range transported aerosol during the wildfire season. In conjunction with negligible local emission sources, this makes PMO an ideal site for the study of long-range transported free tropospheric aerosol.

The Azores-Bermuda anticyclone, causing persistent downward mixing from the upper free troposphere and lower stratosphere, is the dominant meteorological pattern in this region, and strengthens in the summer (Zhang et al., 2017). The

FLEXible PARTicle dispersion model (FLEXPART) retroplumes discussed in Zhang et al. (2017) show that this site is most commonly impacted by North American outflow (30-40%). In the summer months (June – August), 15% of the intercepted air masses have North American anthropogenic influence, and 7.3% have wildfire influence (Zhang et al., 2017). These factors make PMO an excellent site for the study of North American outflow (Val Martin et al., 2008a). In many of the previous studies at PMO, investigators focused on the North American outflows of NO_x, NO_y, CH_4, and O_3 gases (Val Martin et al., 2006; Pfister et al., 2006; Val Martin et al., 2008a; Val Martin et al., 2008b; Helmig et al., 2015) and the physical characteristics of the black carbon aerosol (Fialho et al., 2005; China et al., 2015; China et al., 2017). So far, only Dzepina et al. (2015) has looked at the aerosol bulk chemical characterization and molecular characteristics of the organic aerosol collected at the site.

Recent environmental and laboratory studies have shown that under low temperature and relative humidity conditions aerosol can be in a solid glassy phase (Zobrist et al., 2008; Virtanen et al., 2010). This observation has been hypothesized to lead to longer atmospheric lifetimes for organic species that are otherwise susceptible to degradation through oxidative processes. As an example, polycyclic aromatic hydrocarbons (PAH) such as benzo[a]pyrene were observed to have a much higher ambient concentration than what could be explained by model simulations without considering aerosol phase state (Shrivastava et al., 2017). Recently, PAH have been shown to enhance the formation of a viscous phase state in laboratory generated secondary organic aerosol (SOA) (Zelenyuk et al., 2017). Since PAH are common products of biomass burning and anthropogenic emissions, this enhancement of viscosity could be present in ambient samples as well, leading to a greater likelihood of the occurrence of solid phase aerosol. The solid phase can increase the resistance of aerosol to photodegradation (Lignell et al., 2014; Hinks et al., 2015) and water diffusivity (Berkemeier et al., 2014), which may lead to lower rates of oxidation. Shiraiwa and colleagues developed a set of equations to predict the dry glass transition temperature based on the mass and O/C ratio of organic aerosol components (Shiraiwa et al. 2017; DeRieux et al., 2017). Thus, the phase state of molecular species with respect to ambient conditions can be predicted using the Gordon-Taylor equation (Shiraiwa et al., 2017; DeRieux et al., 2017). Additionally, estimation methods to determine the volatility of organic aerosol were reported by Donahue et al. (2011) and Li et al. (2016). Both the phase state and volatility are potentially important to understand the processes that affect aerosol during transport and aging. The low oxidation observed by Dzepina et al. (2015) was attributed to the dominance of long-lived aerosol that resisted the removal mechanisms, however it is possible that the phase state of the aerosol during transport played a significant role. The increased resistance to photodegradation (Lignell et al., 2014; Hinks et al., 2015) and water diffusivity (Berkemeier et al., 2014) of solid phase organic aerosol provide a basis for this hypothesis.

Ultrahigh resolution mass spectrometry (MS) is a necessary tool for determining the molecular characteristics of complex mixtures such as organic aerosol. It has been used to analyze dissolved organic matter (Kido-Soule et al., 2010; Herzsprung et al., 2014), cloud water (Zhao et al., 2013), fog water (Mazzoleni et al., 2010), sea spray (Schmitt-Kopplin et al., 2012), and organic aerosol (Walser et al., 2007; Mazzoleni et al., 2012; O'Brien et al., 2013; Wozniak et al., 2014; Dzepina et al., 2015). Ultrahigh resolution MS techniques are typically paired with electrospray ionization (ESI) because it is a soft ionization technique with little to no fragmentation of the molecular species being analyzed. Negative mode ESI is sensitive to acidic groups such as carboxylic acids in organic species, which is ideal for the analysis of long-range transported organic aerosol due to its generally acidic nature. The ultrahigh resolution available from Fourier transform ion cyclotron resonance mass spectrometry (FT-ICR MS) and the high field Orbitrap Elite MS instruments (R = 240,000) is used to separate sulfur containing species from carbon, hydrogen, and oxygen containing species (Schmitt-Kopplin et al., 2010), which is important because sulfur containing species are common in atmospheric aerosol (Schmitt-Kopplin et al., 2010; Mazzoleni et al., 2012; Dzepina et al., 2015).

The observations of Dzepina et al. (2015) raised interesting questions regarding the nature of long-range transported free tropospheric aerosol. To further elucidate the detailed molecular characteristics of free tropospheric aerosol, we analyzed three pollution events using ultrahigh resolution FT-ICR MS. We observed key molecular differences in the oxidation related to the transport pathways from comparisons of the detailed molecular composition of the pollution events and their apparent emission sources. In this paper, we present the detailed molecular characteristics of organic aerosol collected at PMO and use the aerosol chemical composition, FLEXPART modeling simulations, and physical property estimates to interpret those characteristics and infer implications for long-range transported organic aerosol.

2 Methods

2.1 Sample collection

$PM_{2.5}$ samples were collected at PMO on 8.5 x 10 in. quartz fiber filter using high volume air samplers (EcoTech HiVol 3000, Warren, RI, USA) operated at an average volumetric flow rate of 84 $m^3 hr^{-1}$ for 24 h. Prior to sampling, the filters were wrapped in clean, heavy-duty aluminum foil and then baked at 500 ^0C for ~8 hours to remove organic artifacts associated with the filters. Afterward, they were placed in antistatic sealable bags until deployment. We deployed four air samplers at the site, each was set up with a filter simultaneously and programmed to start one day after another, allowing for continuous sample collection for up to four consecutive days. This procedure was used to maximize the number of filters collected. Daily visits and maintenance were prohibited by the time consuming and strenuous hike necessary to reach the site. The sampled filters were removed and returned to the same aluminum wrapper and bag. The samples were then brought down the mountain and stored in a freezer until cold transport back to Michigan Tech where they were stored in a freezer until analysis. Three samples, collected in consecutive years at PMO, on 27-28 June 2013, 5-6 July 2014, and 20-21 June 2015 were analyzed in this study. The sampling time for all samples was 24 hours, for 27-28 June sampling began at 19:00, for 5-6 July, and for 20-21 June sampling began at 15:00, all times local.

2.2 Chemical analyses

Organic carbon and elemental carbon (OC/EC) measurements were performed using an OC/EC analyzer (Model 4, Sunset Laboratory Inc. Tigard, OR, USA) following the NIOSH protocol. Major anions and cations were analyzed using ion chromatography. Anion analysis was performed using a Dionex ICS-2100 instrument (Thermo Scientific) with an AS-17-C analytical and guard column set (Thermo Scientific) using a KOH generator for gradient elution. Cation analysis was performed using a Dionex ICS-1100 instrument with CS-12A analytical and guard column set (Thermo Scientific) and an isocratic 20 mM methanesulfonic acid eluent. The instruments were operated in parallel using split flow from the autosampler. Additional details about the analytical and instrumental methods can be found in the Supplement.

2.3 Ultrahigh resolution FT-ICR mass spectrometry analysis

The samples for FT-ICR-MS analysis were selected based on the organic carbon concentration. Selected samples typically had more than 1000 μg of organic carbon per quarter of the quartz fiber filter. Sample preparation was described in detail in previous studies from this group (Mazzoleni et al., 2010, 2012; Zhao et al., 2013; Dzepina et al., 2015). Briefly, one quarter of the quartz filter was cut into strips, placed in a pre-washed and baked 40 mL glass vial, and then extracted using ultrasonic agitation in Optima LC/MS grade deionized water (Fisher Scientific, Waltham, MA, USA) for 30 minutes. The extract was then filtered using a baked quartz filter syringe to remove undissolved material and quartz filter fragments. The sample filter was then sonicated again in 10 mL of Optima LC/MS grade deionized water for 30 minutes, re-filtered and added to the original 30 mL of filtrate, for a total of 40 mL. Ice packs were used during sonication to ensure the water temperature stayed below 25 °C. The water-soluble organic carbon (WSOC) compounds were then isolated using Strata-X (Phenomenex, Torrance, CA, USA) reversed phase solid phase extraction (SPE) cartridges to remove inorganic salts that can adduct with organic compounds

during electrospray ionization. During reversed phase SPE, losses of highly water soluble, low molecular weight organic compounds are expected. The cartridges were conditioned with acetonitrile and LC/MS grade water before all 40 mL of filtrate were put through the cartridges at a rate of roughly 1 mL/min. The compounds retained by the cartridge were eluted off with 2 mL of an aqueous acetonitrile solution (90/10 acetonitrile/water by volume) and stored in the freezer until analysis.

Ultrahigh resolution mass spectrometric analysis was done using FT-ICR MS with ESI at the Woods Hole Oceanographic Institution (Thermo Scientific LTQ Ultra). The samples were analyzed using direct infusion ESI in the negative ion mode. The spray voltage ranged from 3.15 to 3.40 kV depending on the ionization stability with a sample flow rate of 4 to 5 µL/min. We used a scan range of *m/z* 100 – 1000 with a mass resolving power of 400,000 (defined at *m/z* 400) for all samples. The samples were run in duplicate and 200 transient scans were collected. The transients were co-added for each replicate run using the Midas Co-Add tool and molecular formula assignments were done using Composer software (Sierra Analytics), as described in previous studies (Mazzoleni et al., 2012; Dzepina et al., 2015). The resulting molecular formula assignments underwent additional quality assurance (QA) data filtering to make sure the formula assignments were chemically reasonable with respect to O/C, hydrogen to carbon ratio (H/C), double bond equivalent (DBE), and absolute PPM error as described in the Supplemental Information of Putman et al. (2012). To produce the final data set for each sample, the replicates were aligned and only the molecular formulas found in both replicates after QA were retained.

2.4 FLEXPART numerical simulations

FLEXPART modeling was used to determine the sources, ages, and transport pathways of the aerosol samples collected at PMO. FLEXPART backward simulation (also called retroplumes) was driven by meteorology fields from the Global Forecast System (GFS) and its Final Analysis (FNL) with 3-hour temporal resolution, 1° horizontal resolution, and 26 vertical levels. The output was saved in a grid with a horizontal resolution of 1° latitude by 1° longitude, and eleven vertical levels from the surface to 15,000 m a.s.l. FLEXPART retroplumes (upwind distributions of residence time) are multiplied with CO emission inventories from the Emissions Database for Global Atmospheric Research (EDGAR version 3.2 (Olivier and Berdowski, 2001)) and the Global Fire Assimilation System (Kaiser et al., 2012) to estimate the influence from anthropogenic and wildfire sources, respectively. This modeling approach has been used in several PMO studies (e.g., Dzepina et al., 2015; Zhang et al., 2014, 2017). It is an overall powerful tool for the interpretation of the chemical composition in this work.

It addition to the typical FLEXPART modeling done for the site (e.g., retroplume, CO source apportionment), we extracted the ambient temperature and relative humidity from the Global Forecast System (GFS) analysis data for model grids along the FLEXPART simulated transport pathways. These parameters were then used to predict the phase state of aerosol during transport, based on its molecular composition from ultrahigh resolution MS and using estimation methods recently developed by Shiraiwa et al., (2017) and extended to higher masses by DeRieux et al. (2017). The phase state determination method provides new information for the interpretation of the results that we discuss in Sect. 3.5.

3 Results and discussion

3.1 Overview of the aerosol chemistry: OC/EC and IC

In this study, we present the detailed composition of three individual samples collected for 24 hours on 27-28 June 2013, 5-6 July 2014, and 20-21 June 2015 at the PMO. These samples, referred to as PMO-1, PMO-2 and PMO-3 hereafter, were selected after analysis of organic and elemental carbon (OC/EC) were performed for all 127 aerosol samples collected in this study. The selected samples all had elevated organic carbon (OC) concentrations (Table 1) representing the capture of a pollution plume. After blank subtraction, the median OC of the samples collected over the summers of 2013-2015 was 0.16 ± 0.018 µg/m^3. The minimum OC level measured was below the average blank concentration and the maximum was 2.07 ± 0.017

µg/m^3 (PMO-1). The most abundant anions and cations in these samples are also shown in Table 1. The presence of these ions is consistent with the results of other studies (Yu et al., 2005; Aggarwal and Kawamura, 2009). Further discussion of the composition and trends for all the study samples will be presented in a future manuscript.

The concentrations of common anions and cations can offer important insight regarding cloud processing and emission sources of the collected aerosol samples (Table 1). Specifically, the elevated level of sulfate observed in the PMO-2 sample can be an indicator of anthropogenic influence, cloud processing, or marine influence (Yu et al., 2005). We also observed elevated oxalate concentrations in PMO-1 and PMO-2. Oxalate is known to co-vary with sulfate concentrations in the atmosphere when they are formed by aerosol-cloud processing (Yu et al., 2005; Sorooshian et al., 2007). Thus, the oxalate to sulfate ratio can be an indication of cloud processing (Sorooshian et al., 2007) and in general a higher ratio is the result of increased cloud processing. As described in Sorooshian et al. (2007), oxalate concentrations increase with increased cloud processing because there is more time for it to be produced, leading to an increased ratio. PMO-1 had the highest oxalate to sulfate ratio (0.278), followed by PMO-3 (0.124), and PMO-2 (0.084). The observed oxalate to sulfate ratios for these samples are all much higher than what was reported in Sorooshian et al. (2007) suggesting other factors may impact the concentration of these ions. Specifically, an enrichment of oxalate from biomass combustion plumes (Cao et al., 2017) likely contributed to the observed concentrations of these ions in PMO-1 and PMO-3. Generally, increased cloud processing is expected to lead to increased oxidation of atmospheric organic species (Ervens et al., 2008; Zhao et al., 2013), but has also been hypothesized that cloud scavenging of oxidized components could lead to lower overall oxidation by leaving behind reduced aerosol (Dzepina et al., 2015). The bulk concentration of oxalate in PMO-2 is similar to PMO-1, but the sulfate in PMO-2 is much higher, leading to a low oxalate to sulfate ratio. Based on FLEXPART simulations it is likely that PMO-2 underwent aqueous processing (see Sect. 3.5), but high baseline levels of sulfate from possible anthropogenic and marine sources appear to have obscured the oxalate-sulfate relationship (Yu et al., 2005; Sorooshian et al., 2007).

Despite inconsistencies in the replicate potassium measurements for PMO-1, elevated potassium levels were observed, indicating contributions from biomass combustion (Duan et al., 2004). PMO-3 had slightly elevated potassium relative to PMO-2, but not as high as in PMO-1. The nitrate levels in PMO-2 were significantly lower than what was observed in PMO-1 and PMO-3, which is consistent with the observation that the marine boundary layer promotes the rapid removal of HNO_3 (Val Martin et al., 2008b). This is also consistent with removal due to cloud scavenging (Dunlea et al. 2009). The elevated nitrate in PMO-1 and PMO-3 is consistent with the observation of elevated NO_y and NO_x in the plumes of wildfire emissions made in previous studies at PMO (Val Martin et al., 2008a) and a lack of recent cloud scavenging (Dunlea et al. 2009).

Despite the low altitude transport, the major ion concentrations in PMO-2 do not strongly support major influence from marine sources (Quinn et al., 2015; Kirpes et al., 2017). However, the increased concentration of methane sulfonic acid (MSA) in PMO-2 relative to PMO-1 and PMO-3 suggests some degree of marine influence. To estimate this, we used the non-background subtracted sodium concentration to estimate sea salt sulfate according the method described in Chow et al. (2015) this led to a maximum of 25 % of the total sulfate classified as sea salt sulfate.

3.2 FLEXPART retroplume simulation results

The FLEXPART retroplumes for the three samples are shown in Fig. 1. PMO-1 was largely influenced by North American outflow transported relatively high in the free troposphere. Based on the FLEXPART Carbon Monoxide (CO) modeling (Fig. S1), PMO-1 was likely impacted by wildfire emissions from Canada. The transport time for PMO-1 air masses from North America to PMO was about 7 days. The free tropospheric transport is likely due to the high injection heights (Val Martin et al., 2008a) of organic mass from wildfire events in northwestern Quebec (See Fig. S1, S2). Similar events at PMO have been

identified previously by (Val Martin et al., 2008a). The air masses intercepted during PMO-3 were North American outflows that traveled in the lower free troposphere across the Northern Atlantic Ocean to Western Europe before circling back to PMO. The transport time for the PMO-3 air masses from North America to PMO was roughly 10 days. After a northward transport to Western Europe in the jet stream during the first 4-5 days, the simulated plume turned to the south and west, arriving at PMO from Europe in about 2-4 days. This air mass was most likely influenced by wildfire emissions in western and central Canada (U.S. Air Quality, Smog Blog. alg.umbc.edu). Similar to PMO-1, FLEXPART CO source apportionment (Fig. S2) suggests this sample was most influenced by fire, although considering the OC concentration and transport time, it is likely more diluted than what was observed in PMO-1. In contrast, PMO-2 air masses traveled relatively low (≤ 2 km) over the "Rust Belt" (Illinois, Indiana, Michigan, Ohio, Pennsylvania, and New York) of the United States and stayed at approximately the same altitude until it reached the PMO 2-4 days later. This transport pattern suggests that the aerosol was predominantly transported through the boundary layer on its way to the PMO and was primarily influenced by a mixture of continental U.S. anthropogenic and biogenic emissions. This predicted emission source is supported by the FLEXPART CO modeling as well (Fig. S2). The height of the boundary layer over the continent generally ranges from 500-2500 m (Liu and Liang, 2010), which suggests that PMO-2 was within the boundary layer over the United States as well.

3.3 Molecular formula oxidation metrics: O/C and OS_C

In this section, we describe the detailed molecular formula characterization of the three individual samples PMO-1, PMO-2, and PMO-3. Overall, nearly 80% of the observed mass spectral peaks in the ultrahigh resolution mass spectra were assigned molecular formulas, which is comparable to previous studies (Zhao et al., 2013; Dzepina et al., 2015). After removing the duplicate molecular formulas containing ^{13}C or ^{34}S, a total of 3168 (PMO-1), 2121 (PMO-2), and 1820 (PMO-3) monoisotopic molecular formulas remained. Groups of molecular formulas were assigned based on their elemental composition $C_cH_hN_nO_oS_s$, including: carbon, hydrogen, and oxygen (CHO); carbon, hydrogen, nitrogen, and oxygen (CHNO); and carbon, hydrogen, oxygen, and sulfur (CHOS). The most frequently observed compositions were CHO and CHNO. The reconstructed negative ion mass spectra of the monoisotopic molecular formulas for each of the samples are provided in Fig. 2. Considering the ion distribution and normalized relative abundances, PMO-1 and PMO-3 mass spectra look quite similar with a high frequency of individual O/C values < 0.5. This may suggest similar emission sources or aerosol processing. In contrast, PMO-2 has a stronger relative influence of molecular compositions with higher O/C ratios. The O/C histogram plots in Fig. 2 provide additional evidence for the O/C differences between the two types of samples (free troposphere and boundary layer) due to the difference in O/C distribution.

Visual comparison of the mass spectra indicates that PMO-2, which was transported through the North American continental and North Atlantic marine boundary layer, has a prevalence of higher O/C ratio formulas compared to the two samples transported through the free troposphere. It is expected that the samples with longer transport times (PMO-1 and PMO-3) would be more oxidized than a sample with shorter transport time (PMO-2). However, this expectation is based on results from aging studies of secondary organic aerosol (Volkamer et al., 2006; Jimenez et al., 2009) and continental boundary layer anthropogenic aerosol (Mazzoleni et al., 2012; Huang et al., 2014). The lower oxidation observed in the samples transported for a longer time is consistent with the previous study at this site by Dzepina et al., (2015). In fact, when we compared the molecular formula composition of the free tropospheric aerosol sample "9/24" from the study by Dzepina et al. (2015) to the free tropospheric samples in this study (PMO-1 and PMO-3), we observed that 86-91% of the formulas are common. FLEXPART simulations from both works suggest these samples were all affected by wildfire emissions, contributing to their similarity. In contrast, only 75% of the formulas found in the boundary layer sample (PMO-2) were common with those in Dzepina et al. (2015). A comparison with continental boundary layer aerosol (Mazzoleni et al., 2012) finds the opposite trend,

with 78% of the formulas in PMO-2 found to be common with the Mazzoleni et al. (2012) study, compared to 62% of PMO-1 formulas and 76% of PMO-3 formulas. These comparisons can be seen in Table S2.

As observed in the mass spectra and histograms presented in Fig. 2, the samples have noticeable differences in the distribution of O/C values. This is also reflected in the mean O/C values for the samples: 0.47 ± 0.15 (PMO-1), 0.55 ± 0.19 (PMO-2), and 0.46 ± 0.12 (PMO-3). Note that these are averages of thousands of individual measurements, as such the standard deviation represents the range of values and not uncertainties (see Table S3 and Figs. S3-4 for standard errors and violin plots of the distributions). Additional insight was derived from separating the species into CHO, CHNO, CHOS elemental groups. For example, the comparison of the species with CHO formulas in each sample indicates a smaller relative difference between PMO-2 aerosol compared to PMO-1 and PMO-3, with the PMO-2 aerosol having a slightly higher average O/C value (0.51 ± 0.18 (PMO-2) compared to 0.46 ± 0.16 (PMO-1) and 0.45 ± 0.13 (PMO-3)). The smaller difference in O/C is likely reflective of the observation that 85 - 98% of the CHO species in each sample are present in at least one other sample, with 848 (42 - 78%) of the formulas being found in all three samples, as shown in Fig. S5. This suggests that CHO formulas may be fairly uniform throughout the atmosphere, without an abundance of clear marker species after long-range transport, regardless of source region and transport time. This observation may also support those made in other studies which report the decay of marker species after about 24 hours (Bougiatioti et al., 2014; Forrister et al., 2015), because the CHO formulas are often the most abundant group of species and easiest to detect.

In contrast, the CHNO molecular formulas demonstrate clear differences that correlate with the overall O/C ratio. The average O/C value for the CHNO formulas in PMO-2 was 0.58 ± 0.15 compared to 0.48 ± 0.12 in PMO-1 and PMO-3 (Table 2). Differences in the elemental ratios are often visualized using the van Krevelen plot, which shows the correlation of H/C *vs.* O/C. The van Krevelen plot for the three samples with the unique CHNO formulas present in each sample is shown in Fig. 3. Most of the unique CHNO species in PMO-2 (68%) fall in the more oxidized region of the plot, and at high overall O/C values. This differs from the PMO-1 unique species that are predominantly on the less oxidized, low O/C side of the plot, or the oxidized aromatic region. Another observation from the CHNO species is more identified species in both PMO-1 (1120) and PMO-3 (608) than in PMO-2 (561), despite the higher total number of molecular species in PMO-2 compared to PMO-3. This is potentially due to the enrichment of NO_x and NO_y species as previously observed in wildfire pollution events (Val Martin et al., 2008a), which may in turn lead to increased nitrogen content in the organic aerosol species. The nitrogen containing species show a distinct difference in terms of the total oxidation between the two sets of samples, more so than the CHO compounds. This implies that much of the distinction between different aerosol sources may come from heteroatom containing species.

The difference in oxidation is even more evident in the sulfur containing formulas (CHOS). The PMO-2 CHOS species have a much higher average O/C ratio (0.67 ± 0.26) than what is observed in PMO-1 (0.50 ± 0.14). Consistent with the CHNO formulas, the PMO-2 unique CHOS formulas are strongly present (55% of unique formulas) in the oxidized region of the plot, whereas PMO-1 is nearly completely in the less oxidized region of the van Krevelen plot (Fig. S6). The Kendrick plot (Fig. S6c) also demonstrates a clear difference between the two samples. Most of the unique CHOS compounds in PMO-2 are located on the lower mass, higher defect side of the plot, while the PMO-1 formulas are on the higher mass, lower defect side. This difference is due to the larger amount of oxygen present in the PMO-2 formulas, which would lead to a greater mass defect than the more reduced CHOS formulas present in PMO-1. Higher oxygen content of PMO-2 aerosol is supported by its higher O/C ratio when compared to PMO-1 as shown in box plots (Fig. S6d) This is supported by the box plots showing the O/C values for each sample, where PMO-2 has a higher O/C than PMO-1. Very few CHOS molecular formulas (N = 29) were identified in PMO-3 and most of them (N = 26 of 29 total) were also present in PMO-1. Due to the small number of identified

CHOS formulas in this sample we do not consider it in the comparison between CHOS formulas in the samples. The overall differences that are observed in the O/C ratios between the boundary layer transported aerosol (PMO-2) compared to the free troposphere transported aerosol (PMO-1 and PMO-3) highlight the differences in the aging and lifetime of aerosol relative to its transport pathway.

Another commonly used metric of aerosol oxidation is the average oxidation state of carbon (OS_C) described by Kroll et al. (2011). The average OS_C considers the impact of both hydrogen and oxygen for the average oxidation of carbon in each molecular formula (see Equation S1 in the Supplement). The average OS_C values (Table 2) for the three samples show again that PMO-2 is more oxidized than the other two samples. The average OS_C values for the CHO formulas in PMO-1 and PMO-2 are very similar (Table 2), but as shown in the histograms in Fig. 4, their relative abundance distributions are quite different. The OS_C *vs.* carbon number plots in Fig. 4 show some slight differences between PMO-1 and PMO-2, mostly in the distribution of sulfur containing formulas. However, the similarity of the PMO-1 and PMO-3 samples and their difference from the PMO-2 sample is quite clear in the visual comparisons of the histograms of the OS_C values with their normalized relative abundances.

Many of the molecular formulas that show high oxidation ($OS_C > 0$) are present in more than one sample, but the relative abundance of these formulas is lower in the free tropospheric aerosol samples (PMO-1 and PMO-3) compared to the boundary layer (PMO-2) sample. As observed in the mass spectra in Fig. 2, the oxidized species had a higher abundance in PMO-2 than in the other two samples. To support this observation, Table S4 contains the average values of O/C, OS_C, and other characteristics weighted by the relative abundances for each sample. The O/C_w and OS_{Cw} values are increased relative to the unweighted averages in the aerosol transported in the boundary layer (PMO-2), while the aerosol transported in the free troposphere (PMO-1 and PMO-3) does not show much difference between weighted and unweighted averages. This suggests that the oxidized species may be more abundant and important to the overall chemical and physical characteristics of PMO-2 in the atmosphere and may imply higher hygroscopicity, higher cloud condensation nucleation ability (Massoli et al., 2010) and lower volatility (Ng et al. 2011) relative to PMO-1 and PMO-3. The observation of low oxidation in PMO-1 and PMO-3 may support the findings of Aiken et al. (2008) and Bougiatioti et al. (2014) that wildfire aerosol is less oxidized than other types of aged aerosol.

3.4 Molecular formula aromaticity and brown carbon

The aromaticity of the samples is also different between the two groups of aerosol. Based on the aromaticity index (AI; Eq. S2; AI_{mod}; Eq. S3) (Koch and Dittmar, 2006; 2016), the free tropospheric wildfire aerosol samples (PMO-1 and PMO-3) are more aromatic than the boundary layer aerosol (PMO-2) (Fig. 5). The presence of more aromatic species in the long-range transported wildfire aerosol may lead to increased light absorption (Bao et al., 2017) or resistance to oxidation (Perraudin et al., 2006). Aromatic species can also be demonstrative of the presence of brown carbon (BrC; Desyaterik et al., 2013). Aromaticity is heavily dependent on the H/C ratio and the DBE (Eq. S4), where low H/C and large DBE indicate an aromatic structure. Histograms depicting the distribution of H/C and DBE values for the three samples are shown in Fig. S7. As observed for oxidation, PMO-1 and PMO-3 are more similar to each other than they are to PMO-2. Likewise, PMO-1 and PMO-3 exhibit an increase in the number frequency of higher DBE species, which is not observed in PMO-2, supporting the observation of an increased overall aromaticity for free tropospheric aerosol. Many aromatic compounds, such as PAH are known to be carcinogens, and are a product of incomplete combustion biomass burning and anthropogenic emissions (Perraudin et al., 2006; Bignal et al., 2008). Generally, BrC is considered to be aromatic or olefinic in nature (Bao et al., 2017). In our observations, the two samples influenced by wildfire show the greatest amount of olefinic and aromatic species, which could potentially be associated with the presence of BrC compounds. Additional evidence for the presence of BrC in PMO-1 comes from aethalometer measurements using the 7 wavelength aethalometer (Magee Scientific Company, Berkeley, California,

USA) located at the site, which detected a wavelength-dependent peak with an Ångström coefficient of 1.3 during the sampling period. Ångström coefficients above 1 suggest the presence of BrC or iron oxides. Based on the retroplume analysis and comparison to similar samples (Dzepina et al., 2015), the detected peak is very likely the result of BrC (*pers. comm*., Paulo Fialho, 2017). Figure S8 contains the aethalometer observations for this event. Difficulties with the instrument prevented similar data from being collected for PMO-3, though based on the retroplumes, ambient conditions, and molecular characteristics similar results seem likely (*pers. comm*., Paulo Fialho, 2017). This observation may be evidence of long lived BrC species, which is contrary to the suggestion by Forrister et al. (2015) that BrC is mostly removed within 24 hours. Perhaps, the lifetime of BrC is dependent on other factors related to aerosol oxidation and phase state, which we will discuss next.

3.5 Volatility, phase state, and cloud processing: implications for the observed aerosol oxidation

In a recent study, Shrivastava et al. (2017) reported observations of an enhanced lifetime for PAHs due to the aerosol phase state during transport. The aerosol solid phase state has been shown to decrease the rate of photodegradation (Lignell et al., 2014; Hinks et al., 2015) and water diffusivity (Berkemeier et al., 2014). Both photodegradation and water diffusion are expected to strongly affect the oxidation and aging of aerosol species during transport. Additionally, modeling results of Shiraiwa et al. (2017) showed that model SOA is predicted to be solid at altitudes above 2000 m in the northern hemisphere. Volatility can also play a role in the phase state (Shiraiwa et al., 2017). Therefore, we used the parameters reported by Donahue et al. (2011) and Li et al. (2016) to estimate the volatility of aerosol sampled in our study (Figs. S9 and S10, respectively). As expected based on the length of transport for the samples, the majority of formulas show extremely low volatility. Interestingly, when relative abundance was used to color a plot of OS_C *vs.* volatility calculated using the Li et al. (2016) method (Fig. 6), PMO-2 was observed to have more high abundance formulas of extremely low volatility and elevated oxidation relative to PMO-1 and PMO-3. This highlights the correlation between O/C and volatility, where volatility is expected to decrease as O/C increases. We estimated the phase state using the estimation method by DeRieux et al. (2017) for the PMO aerosol and considered it as a possible explanation for the lower than expected oxidation in PMO-1 and PMO-3. The organic aerosol phase state estimation method is based on the glass transition temperature determined from the molecular mass and the elemental O/C ratio along with the ambient temperature and relative humidity. Using the DeRieux et al. (2017) equation (Eq. S5), we found that the CHO molecular formulas in PMO-1 and PMO-3 typically had higher glass transition temperatures than PMO-2, which implies that they would be more solid than PMO-2, given similar atmospheric conditions. We note that although currently the glass transition temperatures can only be estimated for CHO species, the CHO species were the most frequently observed species and constituted the major fraction of the total relative abundance in the PMO samples. Thus, the results are likely to be reasonably representative of the overall aerosol mass and provide an otherwise unattainable estimate of aerosol phase state during transport.

The aerosol phase state during transport was estimated using the Gordon-Taylor equation (Eqs. S6 - S7) with the calculated glass transition temperatures of the identified CHO molecular species and extracted ambient temperature and relative humidity from GFS analysis along the transport pathways using FLEXPART backward simulations. The number fraction of CHO molecular formulas predicted to be liquid, semi-solid, or solid for each sample over the last 5 days of transport is shown in Fig. 7. The prediction was only taken back 5 days due to the increased range of possible meteorological conditions associated with the spread in the air masses as shown in the retroplumes. Another representation of the phase state distributions for the CHO molecular species is shown in Fig. S12. In both figures, PMO-1 and PMO-3 contain a majority of molecular formulas that are predicted to be solid during the transport conditions estimated using GFS analysis. This suggests that a major reason for the low oxidation observed in PMO-1 and PMO-3 is related to the phase state during free tropospheric long-range transport. Solid phase states during transport may also explain the presence of long-lived BrC species in PMO-1, where the BrC species are protected from oxidation similarly to the long-lived PAHs observed by Shrivastava et al. (2017). In contrast to the

observations from PMO-1 and PMO-3, PMO-2 shows a majority of the molecular species to be either semi-solid or liquid during the final 5 days of transport. This indicates an increased susceptibility to oxidation processes in the atmosphere (Shiraiwa et al., 2011), such as aqueous processing. The possibility of aqueous phase processing is supported by the modeled relative humidity in Fig. 7, which is above 50% in PMO-2 for the last 5 days possibly implying the presence of aerosol liquid water, which would likely contribute to aqueous phase processing.

Cloud processing was shown to increase the oxidation of atmospheric organic matter in Zhao et al. (2013) and so aqueous phase oxidation may provide an explanation for the higher oxidation observed in PMO-2 despite its more rapid transport from North America to the PMO. In fact, most of the unique species observed in PMO-2 are in the highly oxidized region of the van Krevelen plot (Fig. 8). Comparing the cloud water composition reported in Zhao et al. (2013) to the uniquely observed species in each of the PMO samples in this study, we saw that most of the species observed uniquely in PMO-2 and the cloud water were highly oxidized (Fig. S13). Since, these highly oxidized species were not observed in either PMO-1 or PMO-3, we hypothesize that their presence indicates aqueous phase oxidation. As mentioned previously, PMO-2 also had a strongly elevated sulfate concentration relative to PMO-1 and PMO-3, which may indicate cloud processing or perhaps marine aerosol contributions. In addition, a strongly elevated oxalate concentration was observed, especially considering the mass of oxalate to the overall organic mass. The organic mass concentration was estimated to be 2 times the OC concentration. In PMO-2, 9.4 % of the organic mass was due to oxalate compared to 2.3 % and 3.0 % in PMO-1 and PMO-3 respectively. Oxalate is also a potential marker of cloud processing (Sorooshian et al., 2007). Furthermore, nitrate is known to be scavenged in cloud processing (Dunlea et al., 2009), leading to its decrease in recently cloud processed aerosol. The nitrate levels in PMO-2 are very low compared to PMO-1 or PMO-3 (Table 1), supporting the idea of cloud scavenging in PMO-2. Overall, the molecular characteristics and major ion concentrations (Fig. S14) indicate that PMO-2 was likely affected by aqueous phase oxidation during transport.

4 Conclusions

Aerosol samples collected on 27-28 June 2013, 5-6 July 2014, and 20-21 June 2015 at the Pico Mountain Observatory were analyzed using ultrahigh resolution FT-ICR mass spectrometry for molecular formula composition determination. FLEXPART retroplumes for the sampled air masses indicate that: (a) PMO-1 and PMO-3 aerosol were transported predominantly through the free troposphere and were influenced by wildfire emissions; and (b) PMO-2 aerosol was transported through the boundary layer over the Northeast continental U.S. and the North Atlantic Ocean before intercepting PMO. Although elevated levels of OC, sulfate, and oxalate were found in all three samples, PMO-2 had the overall highest mass fractions of oxalate and sulfate. PMO-1 and PMO-3 had elevated nitrate and PMO-1 had elevated potassium. The molecular formula assignments indicated differences in the aerosol oxidation between the free troposphere transported aerosol (PMO-1 and PMO-3) and the marine boundary layer transported aerosol (PMO-2). These observations indicate that transport pathways contribute to differences in the oxidation of aerosol. The relative humidity and ambient temperature at upwind times were extracted from the GFS analysis data using FLEXPART and used to estimate the phase state of the aerosol species during transport. These results suggested that aerosols in PMO-1 and PMO-3 were mainly in the solid phase during transport. This would increase their resistance to oxidation and lead to a lower than expected oxidation. This also suggests that biomass burning emissions and BrC injected into the free troposphere are longer-lived than emissions in the boundary layer. PMO-2 was estimated to be mainly semi-solid or liquid, suggesting an increased susceptibility to aqueous phase oxidation relative to PMO-1 and PMO-3, and offering an explanation for the observed increase in oxidation.

Data availability

The molecular formula composition for each sample in this study is available via Digital Commons at the following link: http://digitalcommons.mtu.edu/chemistry-fp/88/.

Acknowledgements

This project was supported with funding from NSF (AGS-1110059) and DOE (DE-SC0006941). Logistical support for the operation of the Pico Mountain Observatory was provided by the Regional Secretariat of the Environment and the Sea of the Portuguese Regional Government of the Azores. Major equipment cost share and graduate student support associated with this project was provided by the Earth, Planetary, and Space Science Institute at Michigan Technological University. We thank Mike Dziobak, Kendra Wright, Sumit Kumar, Andrea Baccarini, Stefano Viviani, Jacques Huber, and Detlev Helmig for assistance in the field. We thank Manabu Shiraiwa, Sarah Petters, and Marcus Petters for helpful discussion regarding aerosol phase state. Finally, we thank Melissa Soule and Elizabeth Kujawinski of the Woods Hole Oceanographic Institution (WHOI) Mass Spectrometry Facility for FT-ICR MS instrument time and assistance with data acquisition (NSF OCE-0619608 and Gordon and Betty Moore Foundation).

References

Aggarwal, S. G. and Kawamura, K.: Carbonaceous and inorganic composition in long-range transported aerosols over northern Japan: Implication for aging of water-soluble organic fraction, Atmos. Env., 43(16), 2532–2540, doi:10.1016/j.atmosenv.2009.02.032, 2009.

Aiken, A. C., DeCarlo, P. F., Kroll, J. H., Worsnop, D. R., Huffman, J. A., Docherty, K. S., Ulbrich, I. M., Mohr, C., Kimmel, J. R., Sueper, D., Sun, Y., Zhang, Q., Trimborn, A., Northway, M., Ziemann, P. J., Canagaratna, M. R., Onasch, T. B., Alfarra, M. R., Prevot, A. S. H., Dommen, J., Duplissy, Metzger, A., Baltensperger, U., and Jimenez J. L.: O/C and OM/OC Ratios of Primary, Secondary, and Ambient Organic Aerosols with High-Resolution Time-of-Flight Aerosol Mass Spectrometry, Environ. Sci. Technol., 42(12), 4478–4485, doi:10.1021/es703009q, 2008.

Bao, H., Niggemann, J., Luo, L., Dittmar, T. and Kao, S.: Aerosols as a source of dissolved black carbon to the ocean, Nat. Commun., 8(1), 510, doi:10.1038/s41467-017-00437-3, 2017.

Berkemeier, T., Shiraiwa, M., Pöschl, U. and Koop, T.: Competition between water uptake and ice nucleation by glassy organic aerosol particles, Atmos. Chem. Phys., 14(22), 12513–12531, doi:10.5194/acp-14-12513-2014, 2014.

Berkemeier, T., Steimer, S., Krieger, U., Peter, T., Pöschl, U., Ammann, M. and Shiraiwa, M.: Ozone uptake on glassy, semi-solid and liquid organic matter and the role of reactive oxygen intermediates in atmospheric aerosol chemistry, Phys. Chem. Chem. Phys., 18(18), 12662–12674, doi:10.1039/c6cp00634e, 2016.

Bignal, K. L., Langridge, S. and Zhou, J. L.: Release of polycyclic aromatic hydrocarbons, carbon monoxide and particulate matter from biomass combustion in a wood-fired boiler under varying boiler conditions, Atmos. Env., 42(39), 8863–8871, doi:10.1016/j.atmosenv.2008.09.013, 2008.

Bougiatioti, A., Stavroulas, I., Kostenidou, E., Zarmpas, P., Theodosi, C., Kouvarakis, G., Canonaco, F., Prevot, A. S. H., Nenes, A., Pandis, S. N. and Mihalopoulos, N.: Processing of biomass-burning aerosol in the eastern Mediterranean during summertime, Atmos. Chem. Phys., 14(9), 4793–4807, doi:10.5194/acp-14-4793-2014, 2014.

Cao, F., Zhang, S., Kawamura, K., Liu, X., Yang, C., Xu, Z., Fan, M., Zhang, W., Bao, M., Chang, Y., Song, W., Liu, S., Lee, X., Li, J., Zhang, G., and Zhang, Y.: Chemical characteristics of dicarboxylic acids and related organic compounds in PM2.5 during biomass-burning and non-biomass-burning seasons at a rural site of Northeast China, Environ. Pollut., 231(Pt 1), 654–662, doi:10.1016/j.envpol.2017.08.045, 2017.

Capes, G., Johnson, B., McFiggans, G., Williams, P. I., Haywood, J. and Coe, H.: Aging of biomass burning aerosols over West Africa: Aircraft measurements of chemical composition, microphysical properties, and emission ratios, J. Geophys. Res-Atmos., 113(D23), doi:10.1029/2008jd009845, 2008.

China, S., Scarnato, B., Owen, R. C., Zhang, B., Ampadu, M. T., Kumar, S., Dzepina, K., Dziobak, M. P., Fialho, P., Perlinger, J. A., Hueber, J., Helmig, D., Mazzoleni, L.R. and Mazzoleni, C.: Morphology and mixing state of aged soot particles at a remote marine free troposphere site: Implications for optical properties, Geophys. Res. Lett., 42(4), 1243–1250, doi:10.1002/2014gl062404, 2015.

China, S., Alpert, P. A., Zhang, B., Schum, S., Dzepina, K., Wright, K., Owen, R. C., Fialho, P. Mazzoleni, L.R., Mazzoleni, C., and Knopf, D. A.: Ice cloud formation potential by free tropospheric particles from long-range transport over the Northern Atlantic Ocean, J. Geophys. Res-Atmos., 122(5), 3065–3079, doi:10.1002/2016jd025817, 2017.

Chow, J. C., Lowenthal, D. H., Chen, L.W.A., Wang, X., and Watson, J. G.: Mass reconstruction methods for PM2.5: a review, Air Qual. Atmos. Hlth., 8(3), 243–263, doi:10.1007/s11869-015-0338-3, 2015.

Collaud Coen, M., Weingartner, E., Furger, M., Nyeki, S., Prevot, A. S. H., Steinbacher, M. and Baltensperger, U.: Aerosol climatology and planetary boundary influence at the Jungfraujoch analyzed by synoptic weather types, Atmos. Chem. Phys., 11(12), 5931–5944, doi:10.5194/acp-11-5931-2011, 2011.

DeRieux, W. W., Li, Y., Lin, P., Laskin, J., Laskin, A., Bertram, A. K., Nizkorodov, S. A. and Shiraiwa, M.: Predicting the glass transition temperature and viscosity of secondary organic material using molecular composition, Atmos. Chem. Phys. Disc., 1–41, doi:10.5194/acp-2017-1066, 2017.

Desyaterik, Y., Sun, Y., Shen, X., Lee, T., Wang, X., Wang, T. and Collett, J. L.: Speciation of "brown" carbon in cloud water impacted by agricultural biomass burning in eastern China, J. Geophys. Res-Atmos., 118(13), 7389–7399, doi:10.1002/jgrd.50561, 2013.

Donahue, N., Epstein, S., Pandis, S. and Robinson, A.: A two-dimensional volatility basis set: 1. organic-aerosol mixing thermodynamics, Atmos. Chem. Phys., 11(7), 3303–3318, doi:10.5194/acp-11-3303-2011, 2011.

Duan, F., Liu, X., Yu, T. and Cachier, H.: Identification and estimate of biomass burning contribution to the urban aerosol organic carbon concentrations in Beijing, Atmos. Env., 38(9), 1275–1282, doi:10.1016/j.atmosenv.2003.11.037, 2004.

Dunlea, E. J., DeCarlo, P. F., Aiken, A. C., Kimmel, J. R., Peltier, R. E., Weber, R. J., Tomlinson, J., Collins, D. R., Shinozuka, Y., McNaughton, C. S., Howell, S. G., Clarke, A. D., Emmons, L. K., Apel, E. C., Pfister, G. G., van Donkelaar, A., Martin, R. V., Millet, D. B., Heald, C. L. and Jimenez, J. L.: Evolution of Asian aerosols during transpacific transport in INTEX-B, Atmos. Chem. Phys., 9(19), 7257–7287, doi:10.5194/acp-9-7257-2009, 2009.

Dzepina, K., Mazzoleni, C., Fialho, P., China, S., Zhang, B., Owen, R. C., Helmig, D., Hueber, J., Kumar, S., Perlinger, J. A., Kramer, L. J., Dziobak, M. P., Ampadu, M. T., Olsen, S., Wuebbles, D. J., and Mazzoleni, L. R.: Molecular characterization of free tropospheric aerosol collected at the Pico Mountain Observatory: a case study with a long-range transported biomass burning plume, Atmos. Chem. Phys., 15(9), 5047–5068, doi:10.5194/acp-15-5047-2015, 2015.

Ervens, B., Cubison, M., Andrews, E., Feingold, G., Ogren, J. A., Jimenez, J. L., DeCarlo, P. and Nenes, A.: Prediction of cloud condensation nucleus number concentration using measurements of aerosol size distributions and composition and light scattering enhancement due to humidity, J. Geophys. Res-Atmos., 112(D10), doi:10.1029/2006jd007426, 2007.

Ervens, B., Carlton, A. G., Turpin B. J., Altieri, K. E., Kreidenweis, S. M., and Feingold, G.: Secondary organic aerosol yields from cloud-processing of isoprene oxidation products, Geophy. Res. Lett., 35(2), doi:10.1029/2007gl031828, 2008.

Ervens, B., Turpin, B. J. and Weber, R. J.: Secondary organic aerosol formation in cloud droplets and aqueous particles (aqSOA): a review of laboratory, field and model studies, Atmos. Chem. Phys., 11(21), 11069–11102, doi:10.5194/acp-11-11069-2011, 2011.

Fialho, P., Hansen, A. D. A. and Honrath, R. E.: Absorption coefficients by aerosols in remote areas: a new approach to decouple dust and black carbon absorption coefficients using seven-wavelength Aethalometer data, J. Aerosol Sci., 36(2), 267–282, doi:10.1016/j.jaerosci.2004.09.004, 2005.

Forrister, H., Liu, J., Scheuer, E., Dibb, J., Ziemba, L., Thornhill, K. L., Anderson, B., Diskin, G., Perring, A. E., Schwarz, J. P., Campuzano-Jost, P., Day, D. A., Palm, B. B., Jimenez, J. L., Nenes, A. and Weber, R. J.: Evolution of brown carbon in wildfire plumes, Geophys. Res. Lett., 42(11), 4623–4630, doi:10.1002/2015gl063897, 2015.

George, I. J. and Abbatt, J. P. D.: Heterogeneous oxidation of atmospheric aerosol particles by gas-phase radicals, Nat. Chem., 2(9), nchem.806, doi:10.1038/nchem.806, 2010.

Helmig, D., Muoz, M., Hueber, J., Mazzoleni, C., Mazzoleni, L., Owen, R. C., Val-Martin, M., Fialho, P., Plass-Duelmer, C., Palmer, P. I., Lewis, A. C. and Pfister G.: Climatology and atmospheric chemistry of the non-methane hydrocarbons ethane and propane over the North Atlantic, Elem. Sci. Anth., 3, 000054, doi:10.12952/journal.elementa.000054, 2015.

Herzsprung, P., Hertkorn, N., Tümpling, W., Harir, M., Friese, K. and Schmitt-Kopplin, P.: Understanding molecular formula assignment of Fourier transform ion cyclotron resonance mass spectrometry data of natural organic matter from a chemical point of view, Anal. Bioanal. Chem., 406(30), 7977–7987, doi:10.1007/s00216-014-8249-y, 2014.

Hinks, M., Brady, M., Lignell, H., Song, M., Grayson, J., Bertram, A., Lin, P., Laskin, A., Laskin, J. and Nizkorodov, S.: Effect of viscosity on photodegradation rates in complex secondary organic aerosol materials, Phys. Chem. Chem. Phys., 18(13), 8785–8793, doi:10.1039/c5cp05226b, 2015.

Huang, R., Zhang, Y., Bozzetti, C., Ho, K., Cao, J., Han, Y., Daellenbach, K. R., Slowik, J. G., Platt, S. M., Canonaco, F., Zotter, P., Wolf, R., Pieber, S. M., Bruns, E. A., Crippa, M., Ciarelli, G., Piazzalunga, A., Schwikowski, M., Abbaszade, G., Schnelle-Kreis, J., Zimmermann, R., An, Z., Szidat, S., Baltensperger, U., El Haddad, I. and Prevot, A. S. H.: High secondary aerosol contribution to particulate pollution during haze events in China, Nature, 514(7521), nature13774, doi:10.1038/nature13774, 2014.

Jimenez, J. L., Canagaratna, M. R., Donahue, N. M., Prevot, A. S. H., Zhang, Q., Kroll, J. H., DeCarlo, P. F., Allan, J. D., Coe, H., Ng, N. L., Aiken, A. C., Docherty, K. S., Ulbrich, I. M., Grieshop, A. P., Robinson, A. L., Duplissy, J., Smith, J. D., Wilson, K. R., Lanz, V. A., Hueglin, C., Sun, Y, L., Tian, J., Laaksonen, A., Raatikainen, T., Rautiainen, J., Vaattovaara, P., Ehn, M., Kulmala, M., Tomlinson, J. M., Collins, D. R., Cubison, M. J., Dunlea, E. J., Huffman, J. A., Onasch, T. B., Alfarra, M. R., Williams, P. I., Bower, K., Kondo, Y., Schneider, J., Drewnick, F., Borrmann, S., Weimer, S., Demerjian, K., Salcedo, D., Cottrell, L., Griffin, R., Takami, A., Miyoshi, T., Hatakeyama, S., Shimono, A., Sun, J. Y., Zhang, Y. M., Dzepina, K., Kimmel, J. R., Sueper, D., Jayne, J. T., Herndon, S. C., Trimborn, A. M., Williams, L. R., Wood, E. C., Middlebrook, A. M., Kolb, C. E., Baltensperger U. and Worsnop D. R.: Evolution of Organic Aerosols in the Atmosphere, Science, 326(5959), 1525–1529, doi:10.1126/science.1180353, 2009

Kaiser, J. W., Heil, A., Andreae, M. O., Benedetti, A., Chubarova, N., Jones, L., Morcrette, J.-J., Razinger, M., Schultz, M. G., Suttie M., and van der Werf, G. R.: Biomass burning emissions estimated with a global fire assimilation system based on observed fire radiative power, Biogeosciences, 9(1), 527–554, doi:10.5194/bg-9-527-2012, 2012.

Kido-Soule, M., Longnecker, K., Giovannoni, S. and Kujawinski, E.: Impact of instrument and experiment parameters on reproducibility of ultrahigh resolution ESI FT-ICR mass spectra of natural organic matter, Org. Geochem., 41(8), 725–733, doi:10.1016/j.orggeochem.2010.05.017, 2010.

Kirpes, R. M., Bondy, A. L., Bonanno D., Moffet, R. C., Wang, B., Laskin, A., Ault, A. P., and Pratt, K. A.: Secondary Sulfate is Internally Mixed with Sea Spray Aerosol and Organic Aerosol in the Winter-Spring Arctic, Atmos. Chem. Phys. Disc., 1–29, doi:10.5194/acp-2017-998, 2017.

Kleissl, J., Honrath, R. E., Dziobak, M. P., Tanner, D., Val Martín, M., Owen, R. C. and Helmig, D.: Occurrence of upslope flows at the Pico mountaintop observatory: A case study of orographic flows on a small, volcanic island, J. Geophys. Res-Atmos., 112(D10), doi:10.1029/2006jd007565, 2007.

Koch, B. P. and Dittmar, T.: From mass to structure: an aromaticity index for high-resolution mass data of natural organic matter, Rapid Commun. Mass Sp., 20(5), 926–932, doi:10.1002/rcm.2386, 2006

Koch, B. P. and Dittmar, T.: From mass to structure: an aromaticity index for high-resolution mass data of natural organic matter, Rapid Commun. Mass Sp., 30(1), 250, doi: 10.1002/rcm.7433, 2016.

Kroll, J. H., Donahue, N. M., Jimenez, J. L., Kessler, S. H., Canagaratna, M. R., Wilson, K. R., Altieri, K. E., Mazzoleni, L. R., Wozniak, A. S., Bluhm, H., Mysak, E. R., Smith, J. D., Kolb, C. E. and Worsnop, D. R.: Carbon oxidation state as a metric for describing the chemistry of atmospheric organic aerosol, Nat. Chem., 3(2), nchem.948, doi:10.1038/nchem.948, 2011.

Laing, J. R., Jaffe, D. A., and Hee, J. R.: Physical and optical properties of aged biomass burning aerosol from wildfires in Siberia and the Western USA at the Mt. Bachelor Observatory, Atmos. Chem. Phys., 16(23), 15185–15197, doi:10.5194/acp-16-15185-2016, 2016.

Lambe, A. T., Onasch, T. B., Massoli, P., Croasdale, D. R., Wright, J. P., Ahern, A. T., Williams, L. R., Worsnop, D. R., Brune, W. H., and Davidovits, P.: Laboratory studies of the chemical composition and cloud condensation nuclei (CCN) activity of secondary organic aerosol (SOA) and oxidized primary organic aerosol (OPOA), Atmos. Chem. Phys., 11(17), 8913–8928, doi:10.5194/acp-11-8913-2011, 2011

Laskin, A., Laskin, J. and Nizkorodov, S.: Chemistry of Atmospheric Brown Carbon, Chemical Reviews, 115(10), 4335–4382, doi:10.1021/cr5006167, 2015

Lee, A. K. Y., Herckes, P., Leaitch, W. R., Macdonald, A. M. and Abbatt, J. P. D.: Aqueous OH oxidation of ambient organic aerosol and cloud water organics: Formation of highly oxidized products, Geophys. Res. Lett., 38(11), n/a-n/a, doi:10.1029/2011gl047439, 2011.

Li, Y., Pöschl, U. and Shiraiwa, M.: Molecular corridors and parameterizations of volatility in the chemical evolution of organic aerosols, Atmos. Chem. Phys., 16(5), 3327–3344, doi:10.5194/acp-16-3327-2016, 2016.

Lignell, H., Hinks, M. and Nizkorodov, S.: Exploring matrix effects on photochemistry of organic aerosols, P. Natl. Acad. Sci., 111(38), 13780–13785, doi:10.1073/pnas.1322106111, 2014.

Liu, S. and Liang, X.: Observed Diurnal Cycle Climatology of Planetary Boundary Layer Height, J. Climate, 23(21), 5790–5809, doi:10.1175/2010jcli3552.1, 2010.

Massoli, P., Lambe, A. T., Ahern, A. T., Williams, L. R., Ehn, M., Mikkilä, J., Canagaratna, M. R., Brune, W. H., Onasch, T. B., Jayne, J. T., Petäjä, T., Kulmala, M., Laaksonen, A., Kolb, C. E., Davidovits, P. and Worsnop, D. R.: Relationship between aerosol oxidation level and hygroscopic properties of laboratory generated secondary organic aerosol (SOA) particles, Geophys. Res. Lett., 37(24), n/a-n/a, doi:10.1029/2010gl045258, 2010.

Mazzoleni, L. R., Ehrmann, B. M., Shen, X., Marshall, A. G. and Collett, J. L.: Water-Soluble Atmospheric Organic Matter in Fog: Exact Masses and Chemical Formula Identification by Ultrahigh-Resolution Fourier Transform Ion Cyclotron Resonance Mass Spectrometry, Environ. Sci. Technol., 44(10), 3690–3697, doi:10.1021/es903409k, 2010.

Mazzoleni, L. R., Saranjampour, P., Dalbec, M. M., Samburova, V., Hallar, A. G., Zielinska, B., Lowenthal, D. H. and Kohl, S.: Identification of water-soluble organic carbon in non-urban aerosols using ultrahigh-resolution FT-ICR mass spectrometry: organic anions, Environ. Chem., 9(3), 285–297, doi:10.1071/en11167, 2012.

Ng, N. L., Canagaratna, M. R., Jimenez, J. L., Chhabra, P. S., Seinfeld, J. H. and Worsnop, D. R.: Changes in organic aerosol composition with aging inferred from aerosol mass spectra, Atmos. Chem. Phys., 11(13), 6465–6474, doi:10.5194/acp-11-6465-2011, 2011.

O'Brien, R. E., Laskin, A., Laskin, J., Liu, S., Weber, R., Russell, L. M. and Goldstein, A. H.: Molecular characterization of organic aerosol using nanospray desorption/electrospray ionization mass spectrometry: CalNex 2010 field study, Atmospheric Environment, 68, 265–272, doi:10.1016/j.atmosenv.2012.11.056, 2013.

Olivier, J.G.J. and Berdowski, J.J.M.: Global emissions sources and sinks, in: The Climate System, Berdowski, J., Guicherit, R. and Heij, B.J., A.A. Balkema Publishers/Swets & Zeitlinger Publishers, Lisse, The Netherlands. 33-78, 2001.

Perraudin, E., Budzinski, H. and Villenave, E.: Kinetic Study of the Reactions of Ozone with Polycyclic Aromatic Hydrocarbons Adsorbed on Atmospheric Model Particles, J. Atmos. Chem., 56(1), 57–82, doi:10.1007/s10874-006-9042-x, 2006.

Pfister, G. G., Emmons, L. K., Hess, P. G., Honrath, R. E., Lamarque, J. F., Val Martin, M., Owen, R. C., Avery, M. A., Browell, E. V., Holloway, J. S., Nedelec, P., Purvis, R., Ryerson, T. B., Sachse, G. W. and Schlager, H.: Ozone production from the 2004 North American boreal fires, J. Geophys. Res-Atmos., 111(D24), doi:10.1029/2006jd007695, 2006.

Pöschl, U.: Atmospheric Aerosols: Composition, Transformation, Climate and Health Effects, Angew. Chem. Int. Edit., 44(46), 7520–7540, doi:10.1002/anie.200501122, 2005.

Putman, A. L., Offenberg, J. H., Fisseha, R., Kundu, S., Rahn, T. A. and Mazzoleni, L. R.: Ultrahigh-resolution FT-ICR mass spectrometry characterization of α-pinene ozonolysis SOA, Atmos. Env., 46, 164–172, doi:10.1016/j.atmosenv.2011.10.003, 2012.

Quinn, P. K., Collins, D. B., Grassian, V. H., Prather, K. A., and Bates, T. S.: Chemistry and Related Properties of Freshly Emitted Sea Spray Aerosol, Chem. Rev., 115(10), 4383–4399, doi:10.1021/cr500713g, 2015.

Rémillard, J., Kollias, P., Luke, E. and Wood, R.: Marine Boundary Layer Cloud Observations in the Azores, J. Climate, 25(21), 7381–7398, doi:10.1175/jcli-d-11-00610.1, 2012.

Schmitt-Kopplin, P., Gelencsér, A., Dabek-Zlotorzynska, E., Kiss, G., Hertkorn, N., Harir, M., Hong, Y. and Gebefügi, I.: Analysis of the Unresolved Organic Fraction in Atmospheric Aerosols with Ultrahigh-Resolution Mass Spectrometry and Nuclear Magnetic Resonance Spectroscopy: Organosulfates As Photochemical Smog Constituents, Anal. Chem., 82(19), 8017–8026, doi:10.1021/ac101444r, 2010.

Schmitt-Kopplin, P., Liger-Belair, G., Koch, B., Flerus, R., Kattner, G., Harir, M., Kanawati, B., Lucio, M., Tziotis, D., Hertkorn, N. and Gebefügi, I.: Dissolved organic matter in sea spray: a transfer study from marine surface water to aerosols, Biogeosciences, 9(4), 1571–1582, doi:10.5194/bg-9-1571-2012, 2012.

Shiraiwa, M., Ammann, M., Koop, T. and Pöschl, U.: Gas uptake and chemical aging of semisolid organic aerosol particles, P. Natl. Acad. Sci., 108(27), 11003–11008, doi:10.1073/pnas.1103045108, 2011.

Shiraiwa, M., Li, Y., Tsimpidi, A., Karydis, V., Berkemeier, T., Pandis, S., Lelieveld, J., Koop, T. and Pöschl, U.: Global distribution of particle phase state in atmospheric secondary organic aerosols, Nat. Commun., 8, ncomms15002, doi:10.1038/ncomms15002, 2017.

Shrivastava, M., Lou, S., Zelenyuk, A., Easter, R., Corley, R., Thrall, B., Rasch, P., Fast, J., Simonich, S., Shen, H. and Tao, S.: Global long-range transport and lung cancer risk from polycyclic aromatic hydrocarbons shielded by coatings of organic aerosol, P. Natl. Acad. Sci., 114(6), 1246–1251, doi:10.1073/pnas.1618475114, 2017.

Sorooshian, A., Lu, M.-L., Brechtel, F., Jonsson, H., Feingold, G., Flagan, R. and Seinfeld, J.: On the Source of Organic Acid Aerosol Layers above Clouds, Environ. Sci. Technol., 41(13), 4647–4654, doi:10.1021/es0630442, 2007.

Tu, P., Hall, W. and Johnston, M.: Characterization of Highly Oxidized Molecules in Fresh and Aged Biogenic Secondary Organic Aerosol, Anal. Chem., 88(8), 4495–4501, doi:10.1021/acs.analchem.6b00378, 2016.

U.S. Air Quality, Smog Blog. alg.umbc.edu, last access: 9 January 2018.

Vakkari, V., Kerminen, V., Beukes, J., Tiitta, P., Zyl, P., Josipovic, M., Venter, A., Jaars, K., Worsnop, D., Kulmala, M. and Laakso, L.: Rapid changes in biomass burning aerosols by atmospheric oxidation, Geophys. Res. Lett., 41(7), 2644–2651, doi:10.1002/2014gl059396, 2014.

Val Martin, M., Honrath, R., Owen, R., Pfister, G., Fialho, P. and Barata, F.: Significant enhancements of nitrogen oxides, black carbon, and ozone in the North Atlantic lower free troposphere resulting from North American boreal wildfires, J. Geophys. Res-Atmos., 111(D23), n/a-n/a, doi:10.1029/2006jd007530, 2006.

Val Martin, M., Honrath, R., Owen, R. and Lapina, K.: Large-scale impacts of anthropogenic pollution and boreal wildfires on the nitrogen oxides over the central North Atlantic region, J. Geophys. Res-Atmos., 113(D17), doi:10.1029/2007jd009689, 2008a.

Val Martin, M., Honrath, R., Owen, R. and Li, Q.: Seasonal variation of nitrogen oxides in the central North Atlantic lower free troposphere, J. Geophys. Res-Atmos., 113(D17), doi:10.1029/2007jd009688, 2008b.

Virtanen, A., Joutsensaari, J., Koop, T., Kannosto, J., Yli-Pirilä, P., Leskinen, J., Mäkelä, J., Holopainen, J., Pöschl, U., Kulmala, M., Worsnop, D. and Laaksonen, A.: An amorphous solid state of biogenic secondary organic aerosol particles, Nature, 467(7317), nature09455, doi:10.1038/nature09455, 2010.

Volkamer, R., Jimenez, J. L., San Martini, F., Dzepina, K., Zhang, Q., Salcedo, D., Molina, L. T., Worsnop, D. R. and Molina, M. J.: Secondary organic aerosol formation from anthropogenic air pollution: Rapid and higher than expected, Geophys. Res. Lett., 33(17), doi:10.1029/2006gl026899, 2006.

Walser, M. L., Desyaterik, Y., Laskin, J., Laskin, A. and Nizkorodov, S.: High-resolution mass spectrometric analysis of secondary organic aerosol produced by ozonation of limonene, Phys. Chem. Chem. Phys., 10(7), 1009–1022, doi:10.1039/b712620d, 2007.

Wozniak, A. S., Willoughby, A. S., Gurganus, S. C. and Hatcher, P. G.: Distinguishing molecular characteristics of aerosol water soluble organic matter from the 2011 trans-North Atlantic US GEOTRACES cruise, Atmos. Chem. Phys., 14(16), 8419–8434, doi:10.5194/acp-14-8419-2014, 2014.

Yu, J. Z., Huang, X., Xu, J. and Hu, M.: When Aerosol Sulfate Goes Up, So Does Oxalate: Implication for the Formation Mechanisms of Oxalate, Environ. Sci. Technol., 39(1), 128–133, doi:10.1021/es049559f, 2005.

Zelenyuk, A., Imre, D. G., Wilson, J., Bell, D. M., Suski, K. J., Shrivastava, M., Beránek, J., Alexander, M. L., Kramer, A. L. and Massey-Simonich, S. L.: The effect of gas-phase polycyclic aromatic hydrocarbons on the formation and properties of biogenic secondary organic aerosol particles, Faraday Discuss., 200, 143–164, doi:10.1039/c7fd00032d, 2017.

Zhang, B., Owen, R. C., Perlinger, J. A., Kumar, S., Wu, S., Val Martin, M., Kramer, L. Helmig, D. and Honrath, R. E.: A semi-Lagrangian view of ozone production tendency in North American outflow in the summers of 2009 and 2010, Atmos. Chem. Phys., 14(5), 2267–2287, doi:10.5194/acp-14-2267-2014, 2014.

Zhang, B., Owen, R. C., Perlinger, J. A., Helmig, D., Val Martín, M., Kramer, L., Mazzoleni, L. R. and Mazzoleni, C.: Ten-year chemical signatures associated with long-range transport observed in the free troposphere over the central North Atlantic, Elem. Sci. Anth., 5, doi:10.1525/elementa.194, 2017.

Zhao, Y., Hallar, A. G. and Mazzoleni, L. R.: Atmospheric organic matter in clouds: exact masses and molecular formula identification using ultrahigh-resolution FT-ICR mass spectrometry, Atmos. Chem. Phys., 13(24), 12343–12362, doi:10.5194/acp-13-12343-2013, 2013.

Zobrist, B., Marcolli, C., Pedernera, D. and Koop, T.: Do atmospheric aerosols form glasses?, Atmos. Chem. Phys., 8(17), 5221–5244, doi:10.5194/acp-8-5221-2008, 2008.

Atmos. Chem. Phys. Discuss., https://doi.org/10.5194/acp-2018-196
Manuscript under review for journal Atmos. Chem. Phys.
Discussion started: 23 February 2018

Atmospheric Chemistry and Physics Discussions

Tables

Table 1. Average concentrations (μg/m^3) of major ions and organic carbon.

Component	PMO-1	PMO-2	PMO-3
Formate	0.0289 ± 0.0003	0.00438 ± 0.00007	0.0119 ± 0.0001
MSA	0	0.00439 ± 0.00006	0.00232 ± 0.00002
Chloride	0.0104 ± 0.0003	0	0.0310 ± 0.0001
Nitrate	0.189 ± 0.002	0.0173 ± 0.0004	0.3010 ± 0.00028
Sulfate	0.338 ± 0.004	1.07 ± 0.01	0.421 ± 0.003
Oxalate	0.0938 ± 0.00070	0.0897 ± 0.00181	0.05222 ± 0.00002
Sodium	0.2101±0.0004*	0.2560±0.0001*	0.548±0.005*
Ammonium	0.1364 ± 0.0004	0.2394 ± 0.00001	0.1193 ± 0.00062
Potassium	0.0791 ± 0.0020**	0.0126 ± 0.0002	0.0197 ± 0.0003
OC	2.07 ± 0.02	0.478 ± 0.026	0.87 ± 0.10

*Sodium concentrations were not background subtracted due to inconsistent and high blank levels, they are included to provide an upper bound on the approximate sodium concentrations.

**Replicate measurements of potassium were inconsistent. The sample could not be re-analyzed because there was no remaining sample. Standard deviation was determined by looking at the average standard deviation of 36 potassium measurements in other samples. This sample should only be considered as elevated potassium and only minimal importance placed on the actual measured value.

Table 2. Molecular formula composition average values and number for each elemental group.

Sample	Group	O/C	H/C	DBE	OS_C	Number
PMO-1	CHO	0.46 ± 0.16	1.28 ± 0.32	8.16 ± 3.68	-0.36± 0.50	1848
PMO-2	CHO	0.51 ± 0.18	1.37 ± 0.28	6.59 ± 2.79	-0.36± 0.53	1281
PMO-3	CHO	0.45 ± 0.13	1.36 ± 0.28	7.34 ± 3.11	-0.46± 0.45	1183
PMO-1	CHNO	0.48 ± 0.12	1.21 ± 0.24	9.40 ± 3.08	-0.25± 0.36	1120
PMO-2	CHNO	0.58 ± 0.15	1.26 ± 0.18	8.03 ± 2.27	-0.10± 0.34	561
PMO-3	CHNO	0.48 ± 0.09	1.24 ± 0.19	9.08 ± 2.33	-0.28± 0.29	608
PMO-1	CHOS	0.50± 0.14	1.77± 0.19	3.04± 1.61	-0.77± 0.41	200
PMO-2	CHOS	0.67± 0.26	1.61± 0.25	3.89± 2.12	-0.27± 0.60	274
PMO-3	CHOS	0.41 ± 0.10	1.90 ± 0.21	1.72 ± 1.22	-1.1 ± 0.27	29

Atmos. Chem. Phys. Discuss., https://doi.org/10.5194/acp-2018-196
Manuscript under review for journal Atmos. Chem. Phys.
Discussion started: 23 February 2018

Atmospheric Chemistry and Physics Discussions

Figures

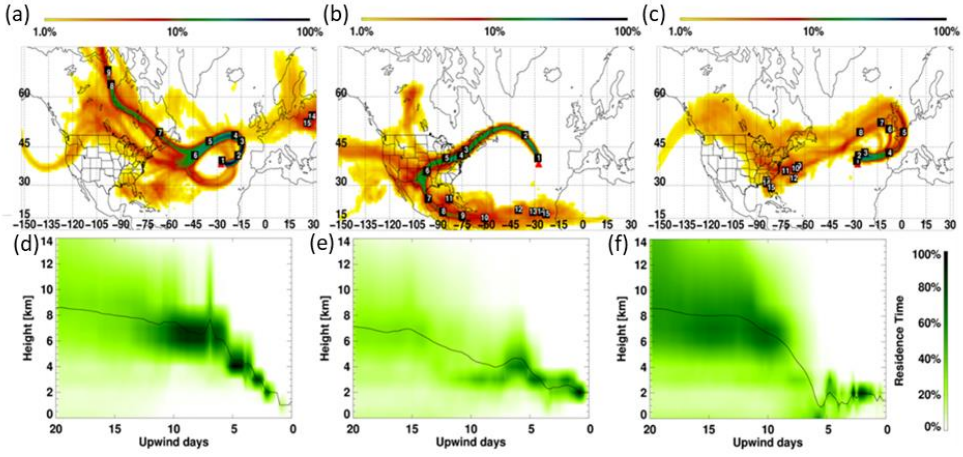

Figure 1. FLEXPART retroplumes for 27-28 June 2013 (PMO-1, (a, d)), 5-6 July 2014 (PMO-2, (b, e)), and 20-21 June 2015 (PMO-3, (c, f): column integrated residence time over the 20-day transport time (a-c) and vertical distribution of the retroplume residence time at given upwind times (d-f). The white labels indicate the approximate locations of the center of the plume for each of the transport days. Residence time is color coded by logarithmic grades representing its ratio to the location of maximal integrated residence time (100%). The black line indicates the mean height of the plume during transport.

Atmos. Chem. Phys. Discuss., https://doi.org/10.5194/acp-2018-196
Manuscript under review for journal Atmos. Chem. Phys.
Discussion started: 23 February 2018

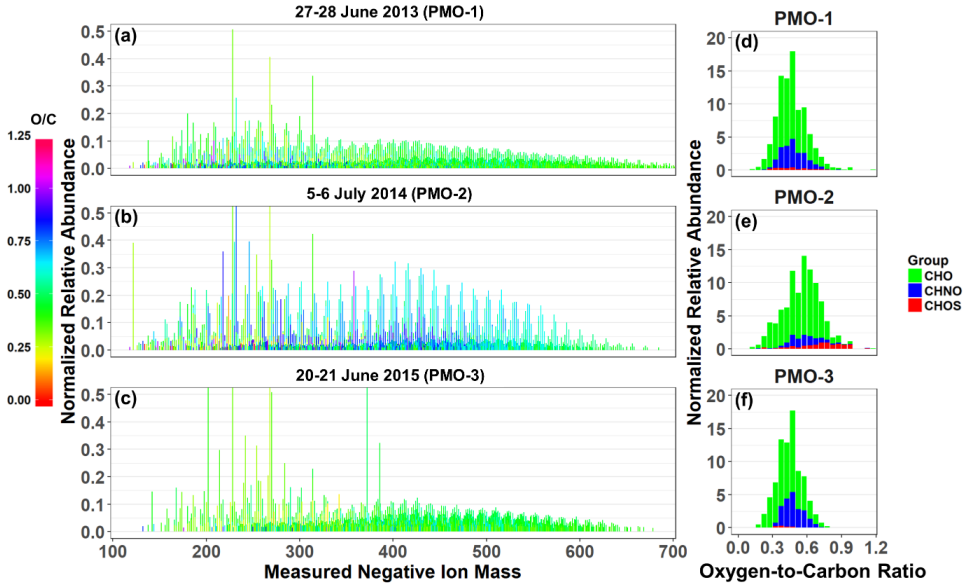

745 **Figure 2.** Reconstructed negative ion mass spectra (a-c) and O/C histograms (d-f) for the three PMO samples. The color in the mass spectra indicates the O/C value for the molecular formula it represents.

750

755

Atmos. Chem. Phys. Discuss., https://doi.org/10.5194/acp-2018-196
Manuscript under review for journal Atmos. Chem. Phys.
Discussion started: 23 February 2018

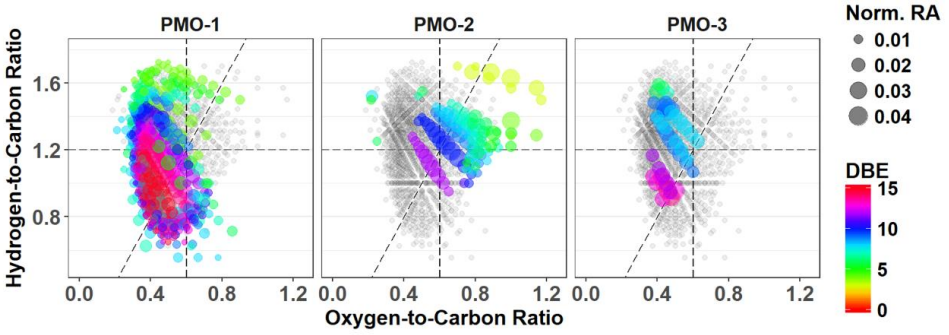

760 **Figure 3.** Van Krevelen plots for the CHNO species with both common species (grey) and unique species (colored). The color represents the number of double bond equivalents in the corresponding molecular formula. The diagonal line is an oxidation line (OS_C = 0; Tu et al., 2016), where the more oxidized formulas are on the right side and less oxidized are on the left.

765

Atmos. Chem. Phys. Discuss., https://doi.org/10.5194/acp-2018-196
Manuscript under review for journal Atmos. Chem. Phys.
Discussion started: 23 February 2018

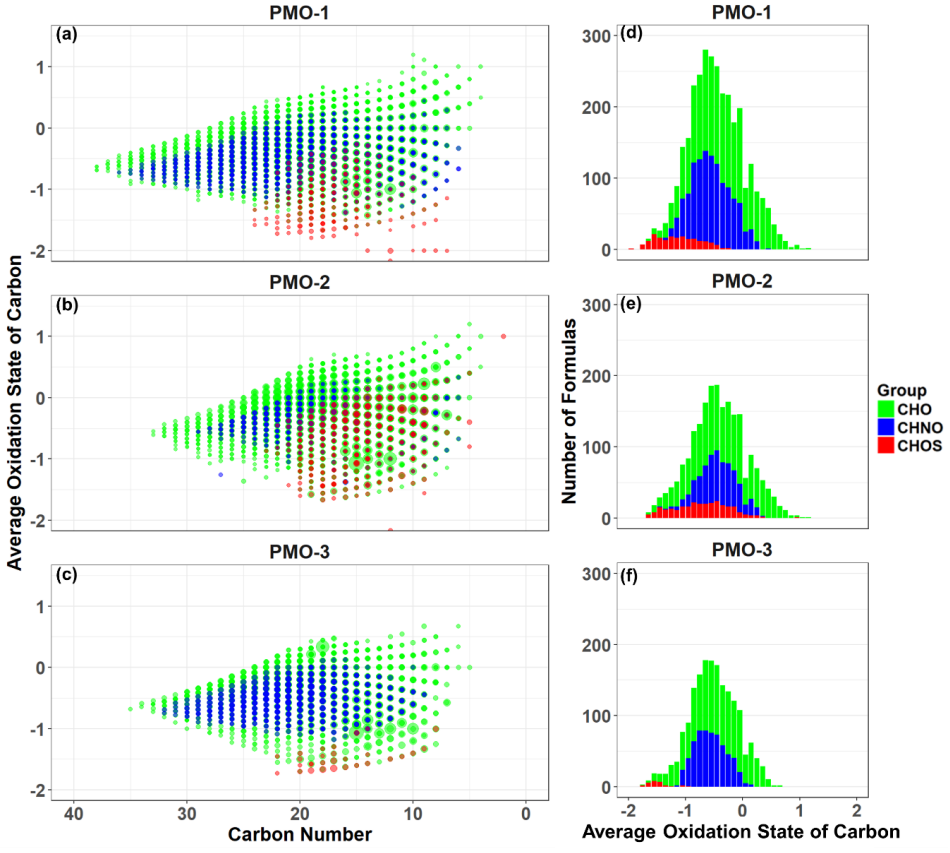

Figure 4. Average OS_C vs. carbon number plots for molecular formula identified in each of PMO samples (a-c). The size of the symbols is scaled to the analyte relative abundance and the color represents the elemental group: CHO (green), CHNO (blue), and CHOS (red). The right panel (d-f) contains average OS_C histograms based on the sum of normalized abundance.

Atmos. Chem. Phys. Discuss., https://doi.org/10.5194/acp-2018-196
Manuscript under review for journal Atmos. Chem. Phys.
Discussion started: 23 February 2018

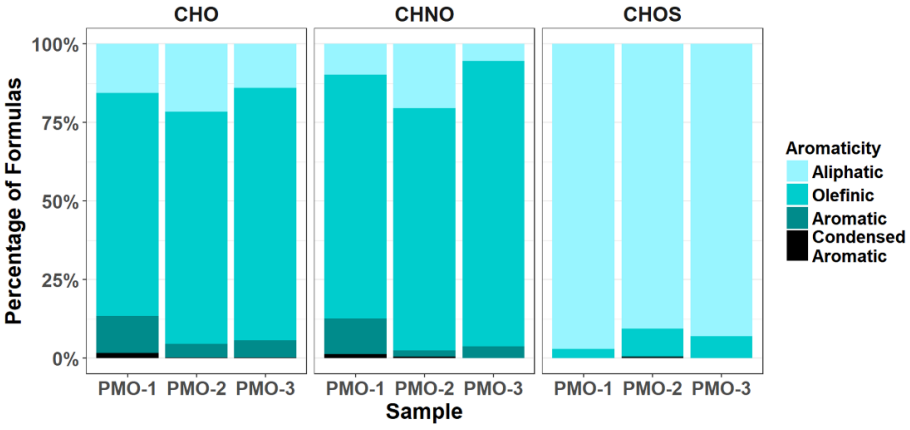

Figure 5. Normalized bar charts for the aromaticity of the three PMO samples, calculated using the Koch and Dittmar (2006; 2016) modified aromaticity index (AI_{mod}).

Atmos. Chem. Phys. Discuss., https://doi.org/10.5194/acp-2018-196
Manuscript under review for journal Atmos. Chem. Phys.
Discussion started: 23 February 2018

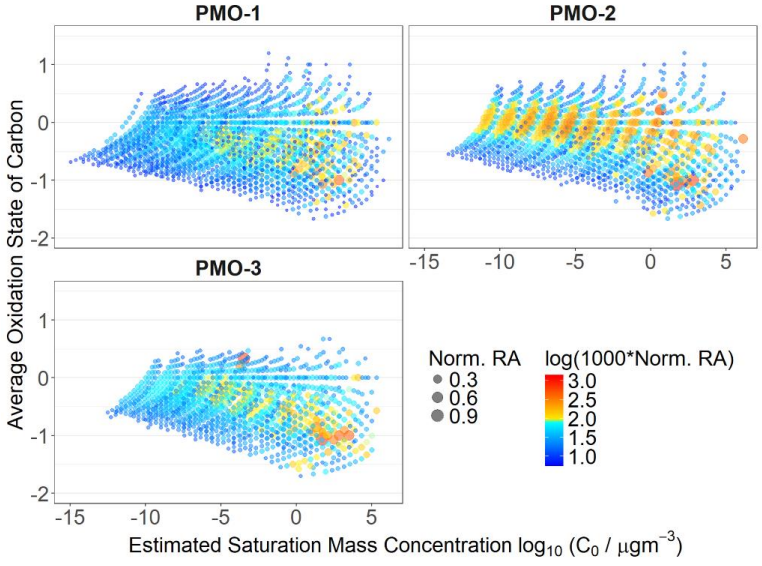

Figure 6. OS_C *vs.* volatility estimated using the Li et al. (2016) method for the CHO species in the three samples. The size is determined by the normalized relative abundance and the color is determined by the logarithm of the normalized relative abundance multiplied by 1000.

785

Atmos. Chem. Phys. Discuss., https://doi.org/10.5194/acp-2018-196
Manuscript under review for journal Atmos. Chem. Phys.
Discussion started: 23 February 2018

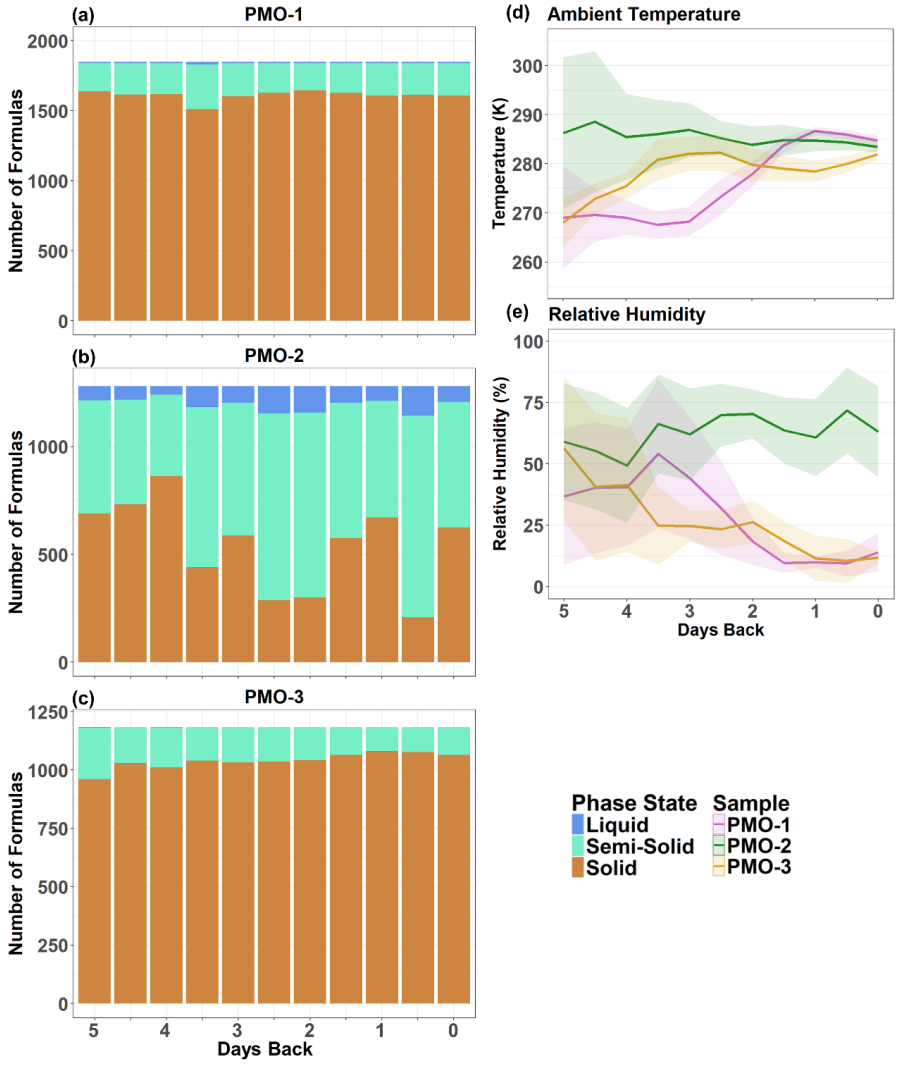

790

Figure 7. Stacked bar charts (a-c) showing the distribution of molecular species by the phase state categories of liquid, semi-solid, and solid for the last five days of transport. Panels d and e show the atmospheric conditions extracted from GFS for the model grids along the FLEXPART simulated transport pathways. The central line is the weighted average and the shading on either side indicates the weighted standard deviation. The results are weighted by residence time.

795

Atmos. Chem. Phys. Discuss., https://doi.org/10.5194/acp-2018-196
Manuscript under review for journal Atmos. Chem. Phys.
Discussion started: 23 February 2018

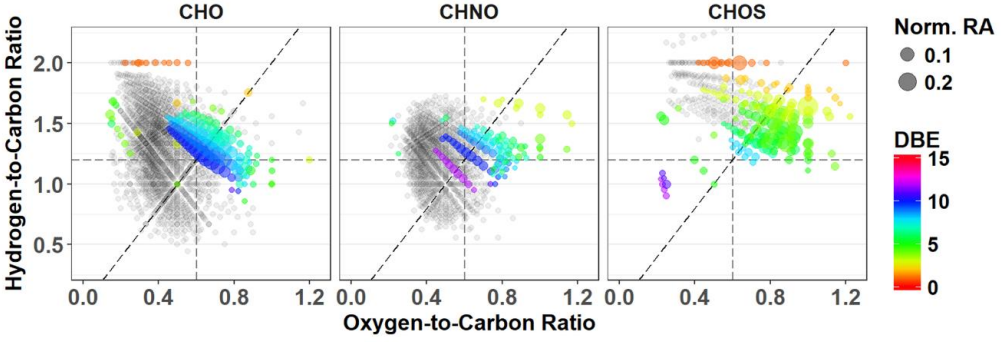

Figure 8. PMO-2 van Krevelen plots for unique molecular formulas separated by group. Symbols are scaled to indicate the normalized relative abundance. The DBE is indicated for each of unique molecular formulas using colored symbols. Common molecular formulas are provided in grey for context.